


Research Article

Design and Characterization of a Traveling-Wave Antenna for Millimeter Applications in the Sub-THz Band

Ndanga Adamou Eric ¹, **Eke Samuel**¹, **Matanga Jacques**¹, **Doka Yamigno Serge**², **Nicolas Corrao**³ and **Tan Phu Vuong**³

¹*Energy Materials Modeling and Methods Research Laboratory (LE3M), Polytechnic Higher National School, University of Douala, Pk. 17 Logbessou 2701, Douala, Cameroon*

²*Department of Physics, Faculty of Science, University of Ngaoundéré, Ngaoundéré 454, Cameroon*

³*IMEP-LAHC UMR CNRS 5130, University of Grenoble Alpes, Grenoble 38016 Cedex1, France*

Correspondence should be addressed to Ndanga Adamou Eric; eric.adamou@gmail.com

Received 14 October 2023; Revised 12 December 2023; Accepted 19 December 2023; Published 30 December 2023

Academic Editor: Mauro Parise

Copyright © 2023 Ndanga Adamou Eric et al. This is an open access article distributed under the Creative Commons Attribution License, which permits unrestricted use, distribution, and reproduction in any medium, provided the original work is properly cited.

The main challenge in manufacturing antennas in the sub-THz band is their small size, which requires adapted manufacturing tools. This paper proposes a uniform linear 3×1 traveling-wave antenna array (ULTWAA) for millimetre applications in the sub-THz band. The designed array allows a continuous beam orientation of $\pm 46.1^\circ$ in the E-plane. A small quarter-wave line added to the ends of the antenna allows the beam to be oriented towards the inside of the antenna, cancelling out surface waves and adapting the impedance to the scanning angle. Thanks to this device, the waves produced are progressive. The antenna manufactured at 100 GHz measures $13 \times 9.7 \times 0.125$ mm. The measured peak gain is 14.2 dBi with 70% bandwidth. For in-phase radiation, the distances between the antenna units have been adjusted, but the adjustment process is tedious due to the interdependence between the antenna units.

1. Introduction

Recently, the terahertz (THz) frequency spectrum, which ranges from 0.1 THz to 10 THz, has been highly valued for its prospective use in multiple applications such as wireless cognition, imaging, spectroscopy, sensing, Industry 4.0, very high precision positioning, and future wireless communications such as 6G [1–4]. The sub-THz frequency band (100 GHz–1 THz), which is currently under testing in many laboratories, has not yet been allocated to specific uses. It has an extremely wide transmission window (bandwidth of ≈ 100 GHz) with manageable losses, and it will be ideal for building wireless links with ultrahigh data rates of up to one terabit per second (Tbps) with super-reliable and minimum latency communications. All of these properties make the sub-THz spectrum the ideal band for sixth-generation (6G) mobile wireless communications [4]. The present work follows from a previous report of the authors [5], who also studied the design and characterization of sub-THz

antennas, with the aim of meeting current and future demand for high-speed communications.

Much work on 6G antenna measurements has been ongoing in recent years, but most of these efforts encounter manufacturing problems because at sub-THz frequencies, the antennas are very small to manufacture [6–8]. Traveling wave antennas could therefore overcome this thorny manufacturing problem because of their large dimensions [9–15]. These antennas use discontinuities in the transmission lines to radiate, and they also have wide bands but generally have low gains. Here, we propose a hollow patch antenna architecture using the commercial simulation tool CST Microwave Studio®. This paper is organized into five parts: the first part motivates our work, and in the second part, we explore the different traveling wave antenna architectures. The results of the simulations are presented in the third part, the fourth part presents the antenna realization and measurement results, and the fifth part concludes the work.

2. Design of Hollow Patch Antenna Elements

2.1. Reflection Suppressing Element. The architecture of an antenna array element is illustrated in Figure 1(a) and consists of a microstrip feed line, two quarter-wave lines, and a rectangular hollow patch. The quarter-wave lines cancel the reflections of port 1 radiated by the antenna so that the traveling wave can be produced on its feed line. The remainder is delivered to port 2, which acts as the input port for the next cascade.

The equivalent circuit of the rectangular patch antenna is given in [9]. Figure 1(b) shows the equivalent electrical model of the patch. The conductance and admittance of the quarter-wave line are represented by G^{pat} and G^{Ltrans} , respectively, with the admittance of the quarter-wave line having a length of 0.25λ . These two values have the reference G_0 , which represents the characteristic admittance of the supply line, in the case where the input impedance of port2 is replaced by a matched load.

To maintain the traveling wave phenomenon along the feed line, the antenna must be well matched to the characteristic impedance of the feed line. The characteristic admittance of the G^{Ltrans} quarter-wave line can be calculated as follows:

$$G^{\text{Ltrans}} = \sqrt{1 + G^{\text{pat}}}, \quad (1)$$

where $G^{\text{pat}} = 1 - S_{11} - S_{12}/S_{12}$.

From (1), the conductance of the G^{Ltrans} line is greater than 1, so the width of the quarter-wave line is always greater than the width of the feed line. The variations in the quarter-wave line admittance as a function of the bandwidth are shown in Figure 2.

The admittance allows us to determine the values of the dimensions (length and width) of the single hollow patch antenna as a function of frequency. After simulation and optimization of the single hollow patch antenna model under CST MWS, we plotted the graph in Figure 2. The work of [9] presents the different steps to obtain all these parameters of the single patch and the antenna array. The value $G^{\text{Ltrans}} = 2.64$ allowed us to obtain the dimensions of the single hollow patch at the resonant frequency of 100 GHz.

2.2. Parameter Research. To design the final structure of our linear uniform traveling-wave antenna array (ULTWAA), we determined the electrical parameters of the reflecting elements, in particular the radiation conductance of the hollow patch G^{pat} , the length of the patch L_{p1} , the length of the feed line L_{p0} , the length of the quarter-wave line L_{q0} , the length of the line connecting the patches in series L_{p2} , the width of the quarter-wave line W_{Lq0} , the width of the feed line W_{p0} , and the width of the patch W_{p1} .

To model the hollow patch antenna, we determined the dimensions of a conventional rectangular patch based on the transmission line equations and then created a hollow in the radiating material. The operating frequency, dielectric constant, and thickness of the substrate were used for predimensioning.

The antenna designed in this work is similar to a filter, mainly the impedance-skipping filter in which we have made hollows in the middle. The difference lies in the design technique used; for microwave filters, Kuroda identities and the Richard transformation are used to determine the dimensions of the stubs to be connected in order to carry out the design, whereas for the antenna, the transmission line equations are generally used to obtain the dimensions of the antenna [15, 16]. Also, for the feed, a traveling wave antenna is fed from one port and the other is connected to earth via a matched impedance, and for a microwave filter, both ports need to be fed. However, their operation is very similar, as the antenna functions as a bandpass filter.

2.2.1. Transmission Line Method. Transmission line theory is used for the determination of the physical dimensions, and several steps of the method are presented as follows [16]:

Step 1: Calculation of the width W of the patch antenna.

The width W of the rectangular patch antenna is given by the following relation:

$$W = \frac{C}{2f_o \sqrt{(\epsilon_r + 1/2)}}, \quad (2)$$

where f_o is the resonant or operating frequency of the antenna, ϵ_r is the relative permittivity of the substrate, and C is the vacuum velocity.

Step 2: Calculation of the effective dielectric constant of the patch antenna (3).

$$\epsilon_{\text{reff}} = \frac{\epsilon_r + 1}{2} + \frac{\epsilon_r - 1}{2} \left[1 + 12 \frac{h}{W} \right]^{-1/2}, \quad (3)$$

where h is the thickness of the substrate.

Step 3: Calculation of the effective length of the patch antenna (4).

$$L_{\text{eff}} = \frac{C}{2f_o \sqrt{\epsilon_{\text{reff}}}}. \quad (4)$$

Step 4: Calculation of ΔL (5)

$$\Delta L = 0.412h \frac{(\epsilon_{\text{eff}} + 0, 3)((w/h) + 0, 264)}{(\epsilon_{\text{eff}} - 0, 258)((w/h) + 0, 813)}. \quad (5)$$

Step 5: Calculation of the length L of the patch antenna (6).

$$L = L_{\text{eff}} - 2\Delta L. \quad (6)$$

Step 6: Calculation of the dimension of the ground plan

$$(L_g, w_g). \quad (7)$$

The transmission line model is only applicable for an infinite ground plane. However, in practice, a finite ground plane with precise values is used. It is shown that

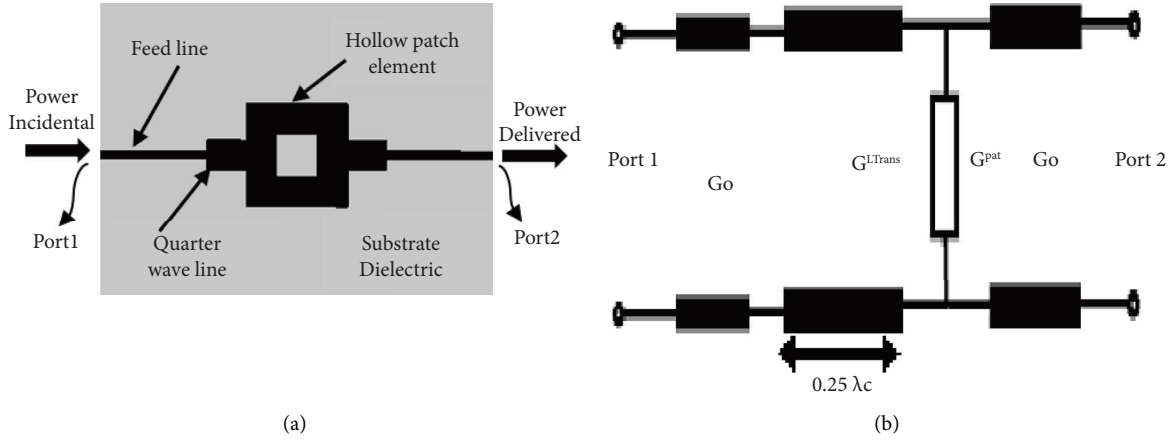


FIGURE 1: The proposed architecture of the element suppresses reflections: (a) architecture; (b) equivalent circuit model.

$$\begin{aligned} L_g &= 6h + L, \\ \omega_g &= 6h + W. \end{aligned} \quad (8)$$

2.2.2. Geometry of the Proposed Antenna. The mutual coupling between the cascaded patches must be considered. In this work, simulation experiments for a uniform network are conducted to obtain all results. The CST simulation software MWS is used. First, a single hollow patch model shown in Figure 3 is used to obtain the initial resonance parameters of our antenna model without considering mutual coupling. All the parameters are presented in Table 1. Then, the configuration of a typical traveling wave antenna consisting of a uniform array of three reflection suppression elements of constant dimensions, shown in Figure 4, is studied and applied to obtain the parameters of the antenna considering mutual coupling.

2.3. Design of a Traveling Wave Hollow Patch Antenna Array. The design of a typical n -element ULTWAA is shown in Figure 4. The radiating elements are sequentially connected by a feed line. Multiple input-multiple output (MIMO) transmission systems are a technology that uses multiple antennas at the transmitter/receiver to improve the throughput, capacity, and coverage of the wireless system [17, 18]. To support the increased throughput of future links and the densification of networks, in terms of the number of users, with the arrival of connected objects, 6G networks will incorporate MIMO systems with a very large number of antennas per base station (e.g., a few dozen to a few hundred).

Figure 4(a) illustrates the structure of a linear antenna array centrally excited by a traveling wave-feeding network.

The proposed array consists of $3N$ elements. It is capable of maintaining the desired radiation pattern, unlike a resonant array, which introduces much more scope for radiation

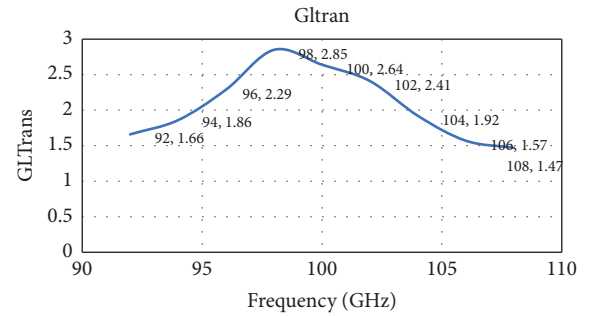


FIGURE 2: Admittance of the quarter-wave line.

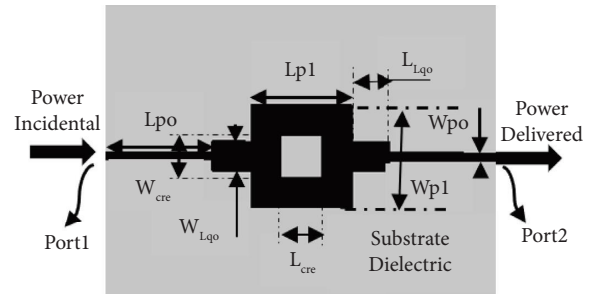


FIGURE 3: Simulation model of the proposed single hollow patch antenna with a traveling wave.

TABLE 1: Detailed dimensions of the single patch.

Parameter	Value (mm)
L	11.55
L_{p0}	3.95
L_{p1}	1.20
L_{q0}	0.80
L_{cre}	1.042
W	13
W_{p0}	0.18
W_{p1}	0.50
W_{Lq0}	0.50

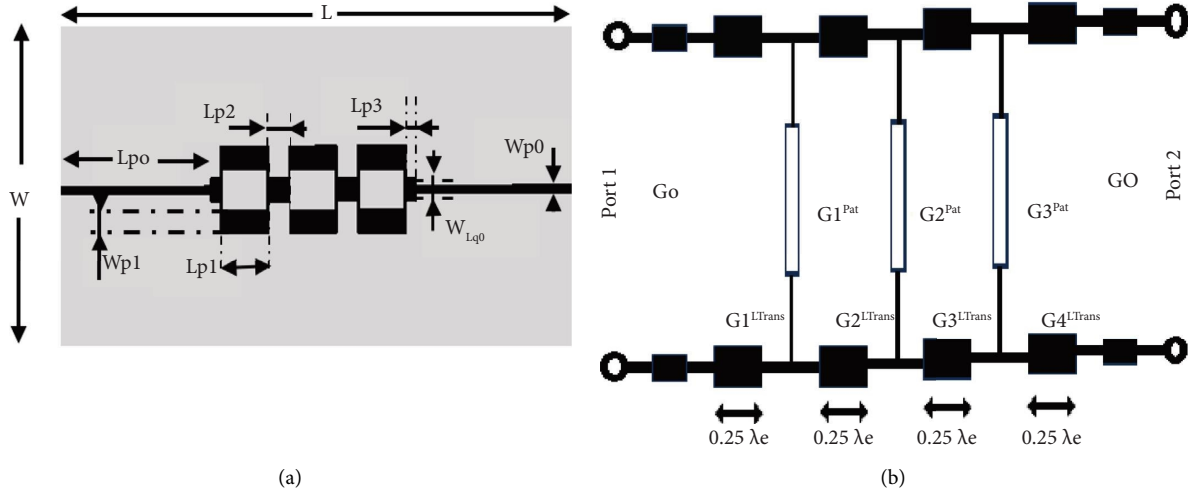


FIGURE 4: Proposed traveling wave antenna array: (a) architecture; (b) equivalent circuit model.

pattern deterioration. In addition, the traveling-wave feed structure offers a fairly wide bandwidth and high efficiency, which is preferable for remote sensing applications. Two $\lambda g/2$ open circuit stubs are added to the array to reflect the power traveling toward the ends.

The input power is delivered through the feed line of port1 or port2 and then radiated through the cascaded elements. In the case of the reflecting elements, the traveling waves are maintained through the supply line regardless of the amplitude and excitation phase. Therefore, we propose that a flexible radiation pattern can be obtained by this ULTWAA. The antenna array architecture proposed in Figure 4 is printed on a Rogers RT5880 dielectric substrate (relative dielectric constant $\epsilon_r = 2.2$ and loss tangent $\tan\delta = 0.0009$) with a thickness of 0.125 mm. The power line with a characteristic impedance of 50Ω , whose width and length are, respectively, $W_{p0} = 0.18$ mm and $L_{p0} = 2.30$ mm, is obtained so that it is suitable for the southwest launch 24359-001J vertical connector used in practice. The parametric study of the proposed base antenna has thus been performed, and the optimized values of each parameter are listed in Table 2 [19, 20].

3. Results and Discussion

The optimization of the proposed antenna dimensions and the simultaneous impedance matching of each port are obtained using a simulator, i.e., the commercially available CST MWS electromagnetic software.

3.1. Electric Field Distribution. Figure 5 shows the electric field distribution in the power network at each port. As shown in Figure 5(a), when feeding port 1, a normal field excited in the transmission line moves to the hollow patches located in the rectangle of the antenna, establishing a surface current of 717 A/m horizontally inside. This field decreases as it progresses toward the load impedance and eventually cancels. When the antenna is fed from port 2 (Figure 5(b)), a normal field excited in the transmission line moves to the

TABLE 2: Detailed dimensions of the patch network.

Parameter	Value (mm)
L	9.7
L_{p0}	2.30
L_{p1}	1.20
L_{p2}	0.50
L_{p3}	0.25
W	13
W_{p0}	0.17
W_{p1}	0.67
W_{Lq0}	0.17
W_{cre}	0.87

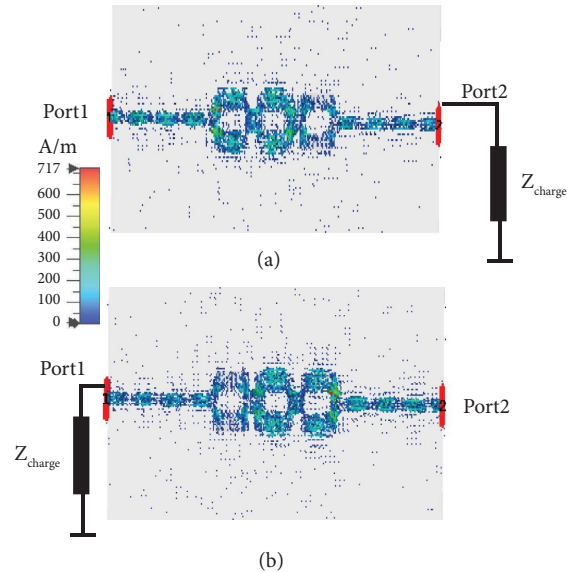


FIGURE 5: Electric field distribution at the power supply ports. (a) Port1. (b) Port 2.

patch in the center of the antenna, establishing an electric field identical to that of the horizontal port1 inside. This electric field gradually diminishes as it propagates to the charging resistor, thus avoiding return waves.

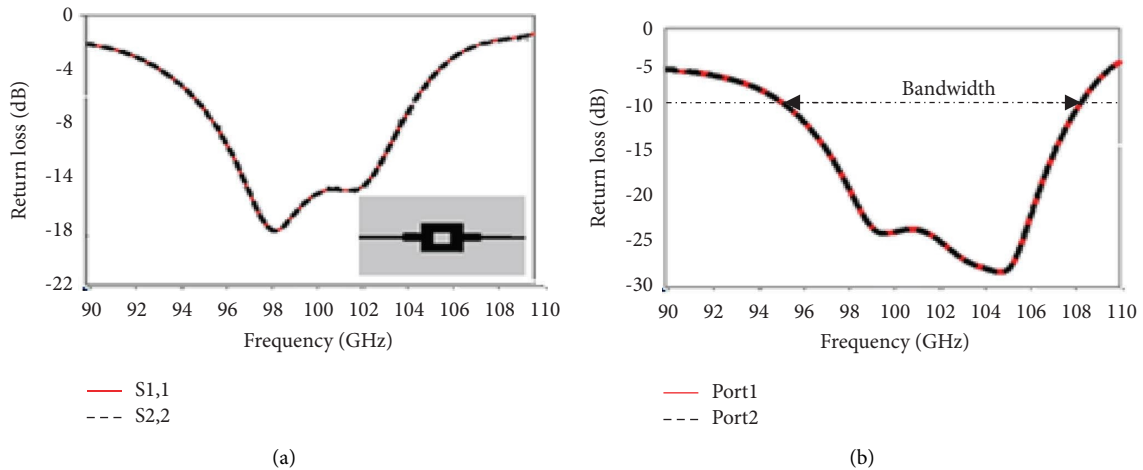


FIGURE 6: Simulated return losses of the proposed antenna: (a) single antenna; (b) patch network.

This distribution of the electric field clearly shows the existence of surface waves that propagate on the surface of the antenna; thus, we have obtained a traveling wave antenna.

3.2. Reflection Coefficient. Figure 6 shows the reflection coefficient of the single matched radiating element. The superposition of the two curves shows that, regardless of which port is fed and the other is connected to an identically matched load, the results are the same. Through optimizations using CST MWS, the radiating element is matched at 50Ω at the center frequency. The bandwidth obtained at -10 dB for the single antenna is 8 GHz (96–104 GHz) (Figure 6(a)).

The hollow patch array obtained the results in Figure 6(b) for each port using the localized port configuration. When we compare the S -parameters obtained at each port, we notice that the results are identical at both ports when one is connected to an identical matched load and the other is fed to a source. The simulation results of the model proposed in Figure 6(b) present a reflection coefficient $S_{11} = -21$ dB with a bandwidth between 96 and 110 GHz or 14 GHz.

3.3. Voltage Standing Wave Ratio (VSWR). The simulation results show good matching of the two ports of the proposed antenna (Figure 7), with the return losses obtained on each port also being identical. The standing wave ratio $VSWR = 1.2:1$ expresses the reasonable level of reflections by the proposed antenna with an impedance of 50 Ohms on each port, while the bandwidth covers 91% of the spectrum band it receives.

3.4. Gain and Directivity and Antenna Efficiency. Figure 8 shows the gain and directivity obtained during the three-dimensional (3D) simulation curve of the antenna.

The gain of our antenna is 12.5 dBi, as shown in Figure 8, and the directivity is 13.6 dBi; the efficiency obtained in this case is 0.92. The radiated efficiency shows that the antenna has 92% of the energy supplied to it at -3 dB.

3.5. Antenna Radiation Patterns. The radiation patterns obtained at 100 GHz during the simulations of the patch network are shown in Figure 9. Figure 5 shows that for the

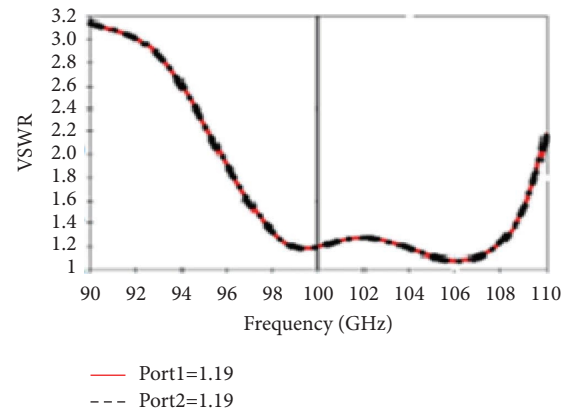


FIGURE 7: Simulated voltage standing wave ratio of the proposed antenna.

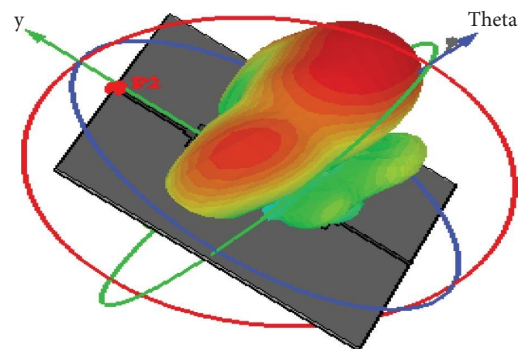


FIGURE 8: 3D radiation diagram.

antenna with the main lobe, the aperture at half power is 48.3° , and for the back lobe, it has an aperture of 31.7° . The results of the different apertures show that the proposed antenna radiates perfectly in the main lobe and that the influence of the back lobes is negligible. The low back radiation pattern of the proposed antenna validates the radiation effect of the antenna, and the mutual coupling power has been radiated perfectly. Several simulations have been

performed, and we observe that with three hollow patches, we obtain satisfactory results because, for example, the actual bandwidth obtained covers 91% of the total bandwidth.

All the results obtained during the simulation are contained in Table 3. The traveling wave-feeding technique helped achieve the required antenna specification.

3.6. Influence of the Number of Hollow Patches. The analysis of the bandwidth presented in Figure 10 of some cascaded hollow patches allowed us to retain our broadband architecture.

The variations in bandwidth and matching impedance as a function of the number of hollow patches are contained in Table 4. We observe good antenna matching and better bandwidth when we have an architecture consisting of three hollow patches. The architectures with 3 and 4 hollow patches in cascade all have good matching, and the difference is in the bandwidth. Nevertheless, we have a very large bandwidth and a better impedance match with the three hollow patch cascade architecture because the actual bandwidth obtained is greater than or equal to 25% of the center frequency.

3.7. Gain Variation as a Function of Antenna Number. Figure 11 shows the gain simulation results for two, three, and four patch antenna arrays. At theta equal to 0° , the three-patch antenna array has 8.05 dBi more gain than the other two antenna architectures. When we look at the graph in Figure 11 at 90° , the three-patch antenna array has a gain of -10.9 dBi, which is also higher than the gains of the other architectures. These results also led us to choose the three-patch cascaded architecture.

4. Experimental Results

4.1. Fabricated Prototype of the Proposed MIMO Antenna. The proposed antenna has been fabricated, as shown in Figure 12(a). In this section, typical near-field antenna performances, such as far-field gain, bandwidth, and S-parameters, are investigated and presented.

Characterization of the miniature microstrip traveling-wave antenna was carried out in an anechoic chamber in the 90–100 GHz band. Southwest launch 24359-001J vertical 1.0 mm connectors at the ports are used to facilitate antenna feeding, and each port is matched by a 50-Ohms load ANRITSU 3656 kit (Figure 12(b)). An ANRITSU 37397D - 2 millimeter-port VNA network analyzer (90–110 GHz band) is used to measure the gain of the reference antennas and the fabricated antenna. The measurement method used is the three-antenna method, in which two identical control antennas are placed at a distance of 370 mm from our antenna (Figure 12(c)). This method allows us to obtain, using three series of measurements, the gains of three different antennas, two of which are identical, and the gain of an unknown antenna.

4.2. Gain Measure. Figure 13 shows the measured gains of the two identical horn antennas, and Figure 14 shows the gain of our antenna. Figure 13 shows that the manufactured

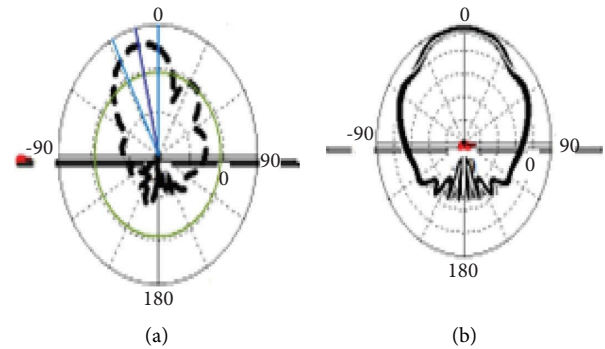


FIGURE 9: Radiation pattern: (a) E-plane and (b) H-plane.

TABLE 3: Summary of the results of the proposed patch network.

Parameters	Values
S_{11} (dB)	-21
S_{22} (dB)	-21
B (GHz)	14
VSWR	1.2
D (dBi)	13.6
G (dBi)	12.5
Opening (AV/AR)	46.1/27.6
η (%)	92

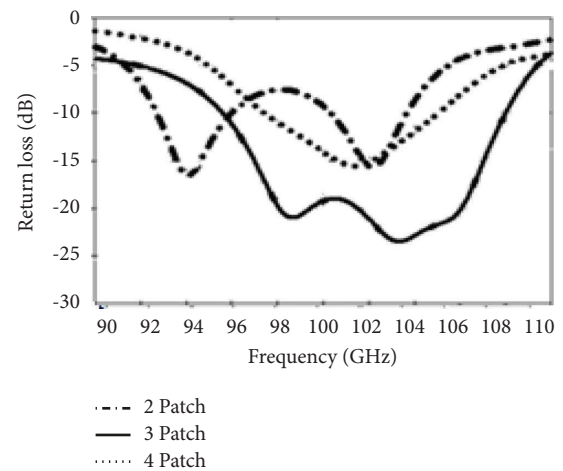
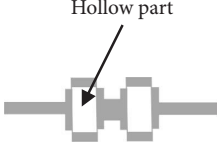
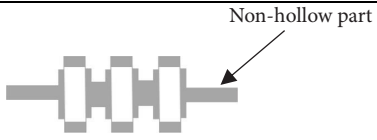



FIGURE 10: Bandwidth variation as a function of cascaded hollow patches.

antenna communicates very well with each of the reference antennas, with a measured gain of 14.2 dBi at 100 GHz. This measured gain is well above that obtained, from which we expected a gain of 12.5 dBi.

4.3. Measurement of S Parameters. To verify the simulation results, an optimal prototype of the antenna presented was built and tested. The amplitudes of four S-parameters were measured, and Figure 15 shows the results of the network analyzer measurements. The amplitude values measured at the working frequency of 100 GHz for the proposed antenna correspond to the following values in dB: $S_{11} = -17.7$ dB, $S_{22} = -10.4$ dB, and $S_{12} = S_{21} = -0.54$ dB. The low value of

TABLE 4: Architectures' comparison.

Number of hollow patches	Architecture	Z (Ω)	B (GHz)
2		54	3.28
3		50	14
4		49.16	7.4

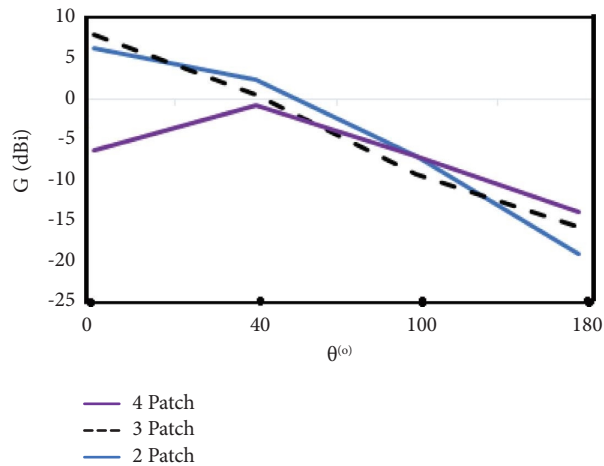


FIGURE 11: Gain variation as a function of antenna number.

S_{22} compared to i_{11} effectively shows that the antenna's port 2 is connected to a matched load of 50 ohms. In addition, the low values of $S_{12} = S_{21}$ express the maximum power transfer between the fed port and the one connected to the load, demonstrating that the antenna radiates efficiently from the fed port to two-thirds of the whole antenna, as shown in Figure 5. These values adequately describe the operation of a traveling-wave antenna.

Figure 16 shows the measurement and simulation results for S_{11} as a function of frequency on the same graph. As shown in Figure 16, the measured and simulated 10 dB bandwidths are 96–110 GHz (70%) and 95.92–109.68 GHz (68.8%), respectively. All simulated and measured S-parameters in decibels at 100 GHz are shown in Table 5.

Indeed, the power cable and SMA connector have a clear impact on the measurement results, which are not considered in the simulation model. Ultimately, both the measurement and simulation results validate the presented design.

4.4. Isolation. The variation in isolation for both ports as a function of frequency is illustrated in Figure 17. Mutual coupling is an electromagnetic phenomenon that can occur in antenna arrays. It occurs due to the electromagnetic interactions produced by each antenna in the array. Most of this radiation is unwanted because the energy produced that would normally be radiated is absorbed by neighboring antennas. Mutual coupling reduces the efficiency and radio performance of the antennas in the array, so the distance between each antenna must be carefully chosen.

4.5. Phase Shifting. The phase shift between ports 1 and 2 of the proposed antenna was measured.

For the phase shift, Figure 18 shows the phase shift between the input and output ports. The signal at the input of port 1 arrives with a delay of 42.8° at port 2 and vice versa. This delay reflects the existence of an energy transfer between the two ports. The port wavelengths at the input and output ports are 0.066 m and 0.054 m, respectively.

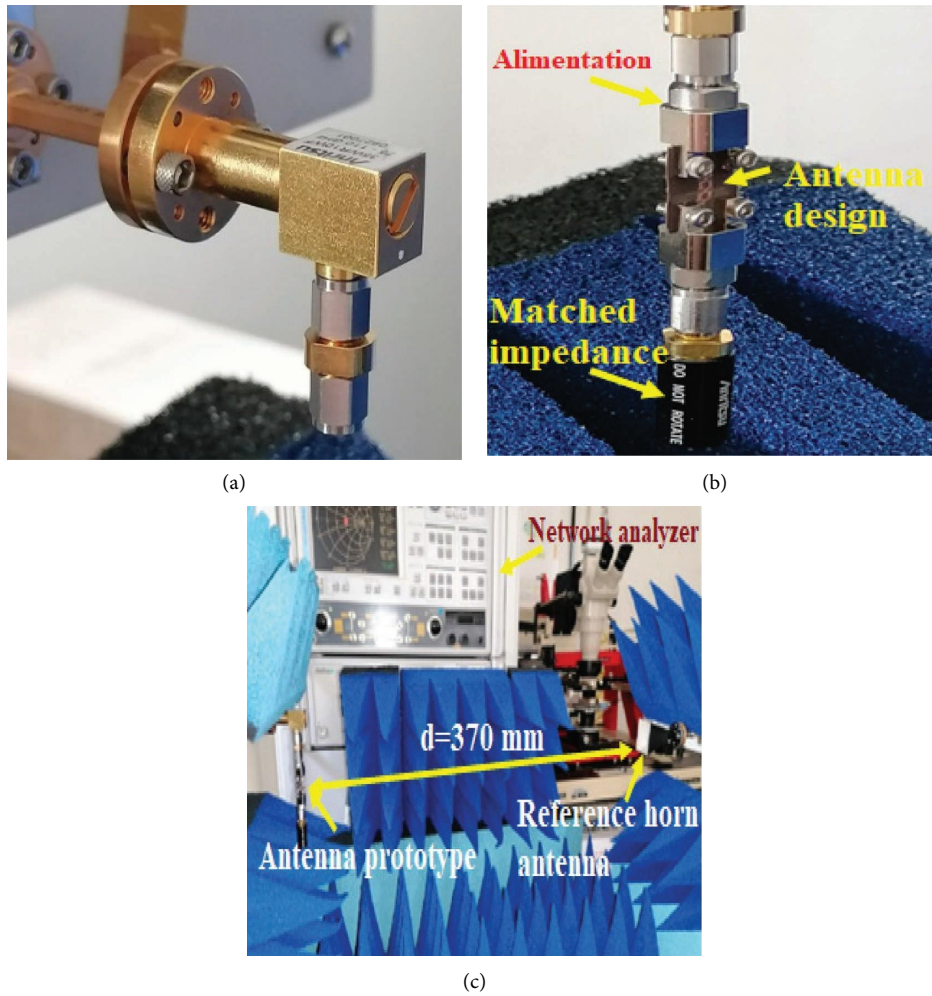


FIGURE 12: Fabrication and measurement for proposed microstrip patch travelling antennas: (a) fabricated traveling antenna. (b) Coaxial waveguide transition. (c) Experimental test which was set up of proposed antennas in an anechoic chamber.

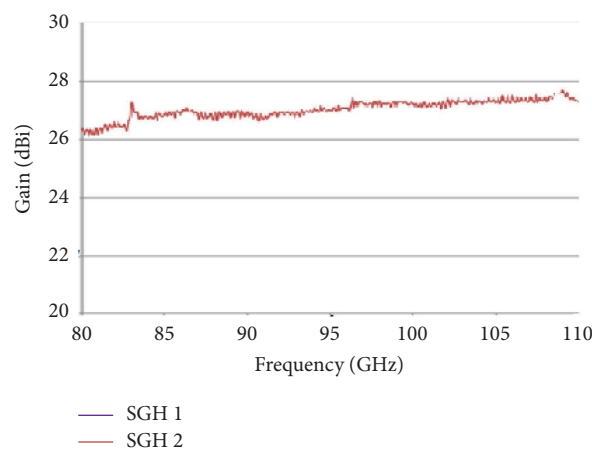


FIGURE 13: Standard gain horn (W band).

Measuring this phase shift demonstrates the functionality of a traveling-wave antenna, with propagating waves that travel efficiently.

Table 6 compares our work with similar reports in the literature. Notably, our antenna has a fractional bandwidth of 70%, which is much larger than that offered by our predecessors.

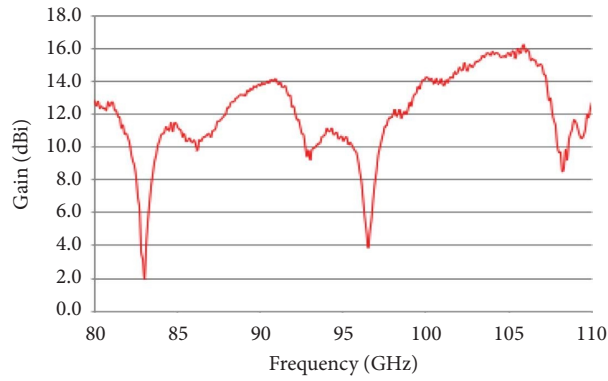


FIGURE 14: Gain of printed antenna.

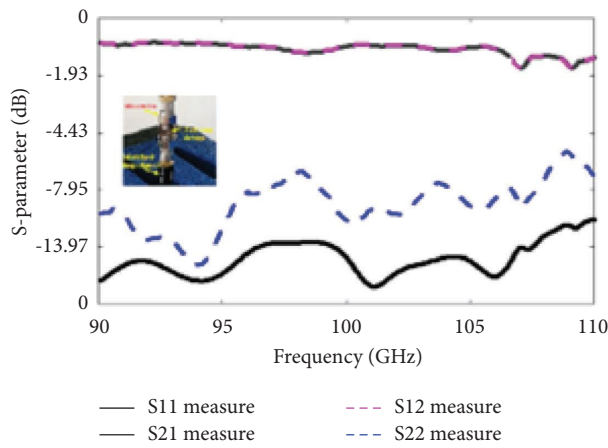


FIGURE 15: Measured S parameters.

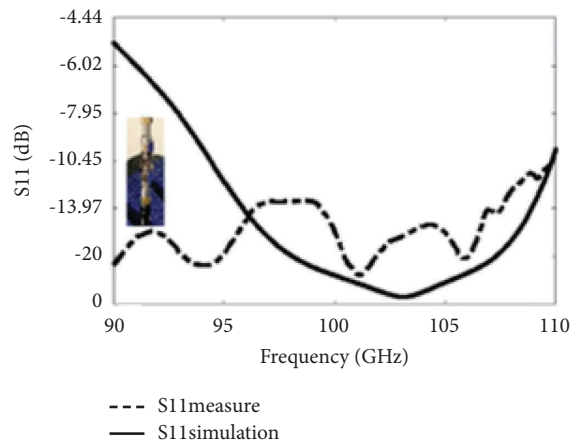


FIGURE 16: S-parameter measurements and simulations.

TABLE 5: Comparison of simulated and measured results at 100 GHz.

Parameters	Simulations	Measures
G (dBi)	12.5	14.2
S11 (dB)	-21	-17.7
IBW (%BP)	69	70

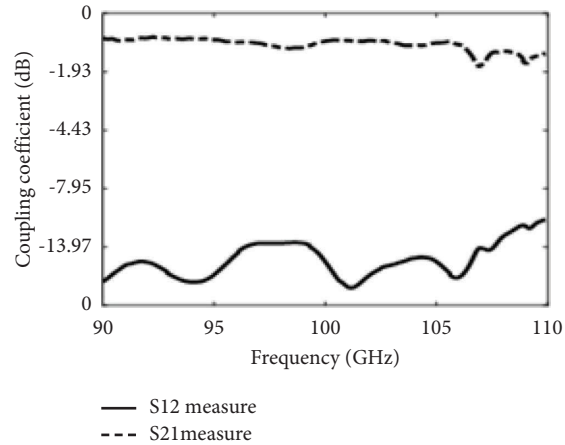


FIGURE 17: Isolation measurement of the antenna proposed.

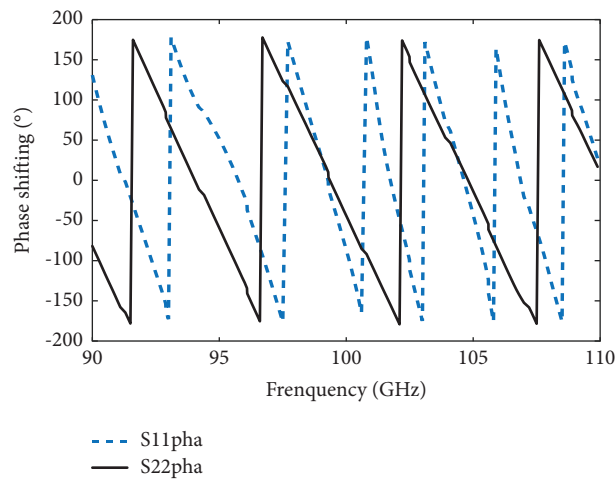


FIGURE 18: Phase shift between antenna ports 1 and 2.

TABLE 6: Comparison between recent papers and this work in the millimeter and microwave bands.

Ref	Frequency, bandwidth, BW [GHz]%	Dimensions in mm	Application	Gain (dBi)	Materials	Implementation	Date of publication
Proposed in this paper	100, [90–110], 70	$13 \times 9.70 \times 0.125$	Millimeter-wave	14.2	RTDuroid5880	CST MWS fabrication	2023
[18]	93, [90–96], 60	Not mentioned	MPT system	13.2	PCB/RT duroid5880 and rogers PCB/RT duroid4003	HFSS	2022
[21]	81, [75–95], 12.5	Not mentioned	Not mentioned	7.82	TGSV surfaces	HFSS fabrication	2021
[22]	84, [75–110], 23	$9.3 \times 9.3 \times 0.4$	Millimeter-wave	14.2	LTCC	HFSS fabrication	2014

5. Conclusion

In this paper, we present an easy-to-implement broadband traveling wave antenna architecture for 6G Sub-THz applications based on hollow patches. Simulation results show that the antenna has a wide bandwidth and is very well suited to 6G applications. This antenna can also be fed from many ports by loading a matched load at the end of a transmitting one, which would give the same results for the same load. We also observed that the number of

cascaded hollow patches influences the bandwidth of the architecture and that it is with three patches that we obtain better adaptation performances. Experimental measurements later confirm the simulation results that we had initially obtained.

Data Availability

The data used to support the findings of this study are included in the article.

Conflicts of Interest

The authors declare that they have no conflicts of interest.

Acknowledgments

The authors would like to thank the head of the IMEP-LaHC research laboratory, Professor Anne KAMINSKI-CACHOPO, for the help with measurements in the electromagnetic and measurement laboratory. The work was carried out thanks to the head of the IMEP-LaHC research laboratory, Professor Anne KAMINSKI-CACHOPO, through their thesis supervisor, Professor T.P. Vuong, because in our country, we do not have funding for the thesis.

References

- [1] W. Long, R. Chen, M. Moretti, W. Zhang, and J. Li, "A promising technology for 6G wireless networks: intelligent reflecting surface," *Journal of Communications and Information Networks*, vol. 6, no. 1, pp. 1–16, 2021.
- [2] X. Lei, M. Wu, F. Zhou, X. Tang, R. Q. Hu, and P. Fan, "Reconfigurable intelligent surface-based symbiotic radio for 6G: design, challenges, and opportunities," *IEEE Wireless Communications*, vol. 28, no. 5, pp. 210–216, 2021.
- [3] Z. Allam and D. S. Jones, "Future (post-COVID) digital, smart and sustainable cities in the wake of 6G: digital twins, immersive realities and new urban economies," *Land Use Policy*, vol. 101, Article ID 105201, 2021.
- [4] T. S. Rappaport, "Wireless communications and applications above 100 GHz: opportunities and challenges for 6G and beyond," *IEEE Access*, vol. 7, pp. 78729–78757, 2019.
- [5] S. Moghe and L. Malviya, "Sub-THz high efficiency MIMO antenna for short range wireless communication," in *Proceedings of the 2022 IEEE 11th International Conference on Communication Systems and Network Technologies (CSNT)*, pp. 66–71, Indore, India, June 2022.
- [6] H. Kanaya, T. Oda, N. Iizasa, and K. Kato, "300 GHz one-sided directional slot array antenna on indium phosphide substrate," in *Proceedings of the 2021 2021 International Symposium on Antennas and Propagation (ISAP)*, pp. 1–2, Hobart, Australia, July 2021.
- [7] Z. Y. Zheng, Z. J. Shao, and J. F. Mao, "A 300-GHz step-profiled corrugated horn antenna array," in *Proceedings of the 2018 IEEE International Symposium on Antennas and Propagation & USNC/URSI National Radio Science Meeting*, pp. 1037–1038, Boston, MA, USA, July 2018.
- [8] A. Dyck, "A 300 GHz microstrip multilayered antenna on quartz substrate," in *Proceedings of the 2018 International Workshop on Antenna Technology 2024 (iWAT)*, pp. 1–3, Nanjing, China, April 2018.
- [9] H. Yi, L. Li, J. Han, and Y. Shi, "Traveling-wave series-fed patch array antenna using novel reflection-canceling elements for flexible beam," *IEEE Access*, vol. 7, Article ID 111466, 2019.
- [10] E. Abdo-Sanchez, D. Palacios-Campos, C. Frias-Heras, F. Y. Ng-Molina, T. M. Martin-Guerrero, and C. Camacho-Penalosa, "Electronically steerable and fixed-beam frequency-tunable planar traveling-wave antenna," *IEEE Transactions on Antennas and Propagation*, vol. 64, no. 4, pp. 1298–1306, 2016.
- [11] M. Alibakhshi-Kenari, M. Naser-Moghadasi, R. A. Sadeghzadeh, B. S. Virdee, and E. Limiti, "Traveling-wave antenna based on metamaterial transmission line structure for use in multiple wireless communication applications," *AEU- International Journal of Electronics and Communications*, vol. 70, no. 12, pp. 1645–1650, 2016.
- [12] C. Min and C. E. Free, "Analysis of traveling-wave-fed patch arrays," *IEEE Transactions on Antennas and Propagation*, vol. 57, no. 3, pp. 664–670, 2009.
- [13] A. R. Diewald and S. Muller, "Design of a six-patch series-fed traveling-wave antenna," in *Proceedings of the 2019 IEEE-APS Conference on Antennas and Propagation for Wireless Communications (APWC)*, pp. 395–399, Granada, Spain, September 2019.
- [14] A. Sarkar, A. H. Naqvi, and S. Lim, "(40 to 65) GHz higher order microstrip-based dual band dual beam tunable leaky-wave antenna for millimeter wave applications," *IEEE Transactions on Antennas and Propagation*, vol. 68, no. 11, pp. 7255–7265, 2020.
- [15] H. Bohra and A. Ghosh, "Design and analysis of microstrip low pass and bandstop filters," *International Journal of Recent Technology and Engineering (IJRTE) ISSN*, vol. 8, 2019.
- [16] A. Sarkar, D. A. Pham, and S. Lim, "60 GHz electronically tunable leaky-wave antenna based on annular surface plasmon polariton media for continuous azimuth scanning," *IEEE Transactions on Antennas and Propagation*, vol. 70, no. 11, pp. 10017–10031, 2022.
- [17] D. Gesbert, M. Shafi, S. Da-Shan, P. J. Smith, and A. Naguib, "From theory to practice: an overview of MIMO space-time coded wireless systems," *IEEE Journal on Selected Areas in Communications*, vol. 21, no. 3, pp. 281–302, 2003.
- [18] A. J. Paulraj, D. A. Gore, R. U. Nabar, and H. Bolcskei, "An overview of MIMO communications—a key to gigabit wireless," *Proceedings of the IEEE*, vol. 92, no. 2, pp. 198–218, 2004.
- [19] A. H. Naqvi, J.-H. Park, C.-W. Baek, and S. Lim, "Via-monopole based Quasi Yagi-Uda antenna for W-band applications using through glass silicon via (TGSV) technology," *IEEE Access*, vol. 8, pp. 9513–9519, 2020.
- [20] A. Lamminen and J. Säily, "Wideband stacked patch antenna array on LTCC for W-band," in *Proceedings of the 5th European Conference on Antennas and Propagation (EUCAP)*, pp. 2962–2966, Rome, Italy, April 2014.
- [21] D. Mathur, S. K. Bhatnagar, and V. Sahula, "Quick estimation of rectangular patch antenna dimensions based on equivalent design concept," *IEEE Antennas and Wireless Propagation Letters*, vol. 13, pp. 1469–1472, 2014.
- [22] L. Liu, "A substrate integrated waveguide-based W-band antenna for microwave power transmission," *Micro-machines*, vol. 13, no. 7, p. 986, 2022.